EUROPEAN ORGANIZATION FOR NUCLEAR RESEARCH

CERN/ISRC/72-32
9 November 1972

PROPOSAL FOR A LARGE 4π CALORIMETER TO INVESTIGATE MULTIBODY EVENTS AT THE ISR

A. Boehm, M. Bozzo, D. Cheng, G. de Zorzi, R. Ellis, H. Foeth, A. Kernan, F. Muller, B. Naroska, C. Rubbia, G. Sette, A. Staude, P. Strolin, L. Sulak, V. Telegdi

III Physikalisches Institut der Technische Hochschule, Aachen.
CERN, Geneva
Harvard University, Cambridge, Mass.
Istituto di Fisica dell'Università di Genova, INFN Sezione di Genova

ABSTRACT

We propose a 4π total absorption calorimeter to measure the number and the energy distribution of particles emitted in the centre of mass. It consists of a large segmented sphere, filled with liquid scintillator. The device offers a genuine 4π geometry, neutral detection, and an easy triggering of events of specific energy distributions. The structure of inelastic events with large transverse momenta can be investigated down to cross-sections of $\sim 10^{-34}$-10^{-36} cm^2.

1. EXPERIMENTAL CONSIDERATIONS

One of the most striking features of the ISR energy range is the spectacular complexity of the events. The average multiplicity is 24 objects, of which $\sim$ 12 are γ's, n, $\bar{n}$, K^o, $\bar{K}^o$, Λ^o, $\bar{\Lambda}^o$, etc. Multiplicities are also subject to large fluctuations. If the recent NAL results[1] are extrapolated on the basis of current theoretical ideas, we expect > 72 object events to occur 1/3000 of all events, or 50 times each second at the design luminosity $L = 4 \times 10^{30}$ cm^2. Still the kinematic limit of the ISR (540 object events, 270 charged π, 270 γ's) is far away. Indeed, since the multiplicity increases like $\sim$ log (S) and the total energy is $\sqrt{S}$, the range of variation of multiplicity becomes much greater than the region we expect to see populated. Higher multiplicty events may contain very specific physics information. For instance, high inelasticity events could be a consequence of very central collisions.

How can we visualize the physics contained, for instance, in a fifty or more prong event ? Single particle spectra, two or more particle correlations of course are very likely averaging over a greater fraction of the information. Evidently the single particle behaviour is probably irrelevant and one must concentrate on more global properties of each event. We believe that density distributions are a significant representation. For instance, we can record at each event the particle distribution $dN/d\Omega$, (charged or neutral) and the energy distribution $dE/d\Omega$. Suppose that a large momentum transfer collision proceeds as an initial scattering between a relatively small number of point-like constituents with subsequent thermodynamical evaporation of the outgoing prongs. The distribution $dE/d\Omega$ is expected to give evidence of clustering along the directions of the scattered constituents (jets) (the "fireball" events described in the cosmic-ray work). Jet behaviour may be limited to specific types

of events, such as large $p_\perp$'s or/and multiplicities. The cross-section could be very small, as suggested by analogies with the deep inelastic scattering of electrons.

One of the most relevant features of the ISR is the possibilitiy of probing large transverse momenta and thus very small distances. Nevertheless, the distribution of elastic scattered protons and of single secondary particles continues to be dominated by low $p_\perp \sim 0.5$ GeV/c, corresponding to distances of ~ 1 fermi, the order of the physical extension of the proton. In fact the distributions fall so fast that it is unlikely that there will be measurable production at the upper part of the $p_\perp$ range available at the ISR. We must find other ways in which the potentially large increase of transverse momenta is directly used. The recent deep inelastic e-p and ν-p experiments have disclosed a whole class of processes which exhibit a true sensitivity to small transverse distances. The common feature of all these processes is that, because of the specific nature of the incident lepton, the whole transverse momentum transferred to the hadrons is observed. The presence of a persisting large cross-section at very large $p_\perp$ is characteristic of inelastic events. This is a striking difference from the elastic channel which, on the contrary, diminishes incredibly fast at increasing $p_\perp$. The phenomenon, usually interpreted as "incoherent" scattering of "point-like" components within the proton, is evidently possible only if break-up of the hadrons is permitted. The electron[2] and neutrino experiments[3] are, of course, observing the very same objects which are colliding with each other at the ISR, and it is interesting to speculate as to whether there exist equivalent processes which one can explore with the extra advantage of the greatly increased centre-of-mass energies of the ISR.

Another likely property of effects related to smallest distances is the very tiny size of the cross-sections. The recent progresses in the luminosity of the ISR coupled with a genuine

4π detection efficiency are bringing cross sections of the order of $1/(4\times10^{30} \times 10^{4}) \approx 2.5\times10^{-35}$ cm^2 into the measurable range of 10 events day. At the design currents of 20A + 20A, (which one might reasonably hope for at the times in which the proposed detector would eventually become operational), 10^{-36} cm^2 correspond to the 1/day level. A main experimental problem is the one of selecting with good efficiency the relevant type of events out of the fantastically large number of p-p interactions. This is possible only provided several physical quantities like transverse momenta, multiplicity etc. are directly accessible to very fast decision-making electronics.

2. THEORETICAL SPECULATIONS : CAN ELECTROMAGNETIC EFFECTS BECOME IMPORTANT AT VERY SMALL DISTANCES ?

Let us consider[4,5] for one moment the diagram in Fig. 1. The dotted line is the photon exchanged in the process

$$p + p \rightarrow X_A + X_B, \qquad (1)$$

where X_A, X_B are multibody final states. The grouping of hadrons in X_A and X_B is made unambiguous by the requirement that the invariant masses M_A and M_B, along with the invariant momentum transfer $-t = q^2 = (P - P_{XA})^2 = (P - P_{XB})^2 > 0$, are made to satisfy : $S >> M_A^2, M_B^2, q^2$.

We make the assumption that the electromagnetic amplitude arises from the one-photon exchange of Fig. 1. Of course, electromagnetic effect will first appear (of order α) by way of interference between the strong and electromagnetic amplitudes. However, in order to determine the size of the purely electromagnetic contributions (of order α^2) to the differential cross-section, we estimate the cross-section of the graph in Fig. 1 in terms of the independently known W_1 and W_2 structure functions which describe electron-proton collisions.

The explicit result, given in Ref. 4, indicates that as long as W_2 (and to a lesser extent W_1) obey scaling, the cross-section for the process (1) falls rather slowly with q^2, that is like $(q^2)^{-2}$. This is instinctively clear since the vertices 1 and 2 exhibit over the scaling region a "point-like" behaviour, with an effective strength of order $\nu W_2 \sim 0.3$. The cross-section is then roughly $(0.3)^2 = 0.1$ of the Mott cross-section. The q^{-4} behaviour is due to the photon propagator. Let us further consider the nature of the states X_A and X_B. Present experimental evidence from e-p collision and theoretical models[6] suggests that there is a "limited fragmentation" type of collision between the virtual photon and the hadron, as seen in the photon-hadron frame of reference. Two particle jets are then generated in the directions of the virtual photon and of the hadron, both characterized by small ($\sim$ 250 MeV/c) transverse momenta in relation to their respective lines of flight. In the case of the ISR, we expect then a four-jet structure, two approximately in the line of the incident protons, and two others, at very large angles, corresponding to the direction of flight of the exchanged photons. Large masses of the states X_A and X_B are then generated by large opening angles between the two jets. The size of the expected cross-sections for Mott scattering are shown in Fig. 2. Rates are well within the potentialities of the ISR up to spectacular values of q^2.

Of course it is by no means obvious that the strong interactions would continue to drop exponentially with q^2, becoming eventually so weak as to be overtaken by electromagnetic diagrams. The same mysterious effect which produces strong-interaction damping may of course suppress also the electromagnetic contributions. Alternatively, as suggested by Berman and Jacob[7], a "strong" analogue of the photon exchange diagram exists, which would lead to "deep inelastic-like" phenomena at cross-sections of several orders of magnitude greater. In this situation electromagnetic effect would remain negligible for ever, away from the exact forward direction (i.e. $q^2 \to 0$, Coulomb region).

Evidently if the deep inelastic behaviour is due to point-like constituents inside the proton it is very reasonable to expect that they interact strongly rather than electromagnetically with each other. In the extended Vector Dominance Model of Sakurai[8] used to explain the deep inelastic behaviour, the higher mass vector mesons are expected to interact strongly, without being mediated by the photon.

Again the deep inelastic behaviour would appear with cross sections orders of magnitude larger than the predictable electromagnetic process.

3. THE EXPERIMENTAL SET-UP

We want to design a detector with the following characteristics :

i) Be able to provide a good measurement of the energy distribution of all hadrons, irrespectively of the charge, nature or number of particles.

ii) An acceptance solid angle as close as possible to 4π.

iii) Triggering of the data recording is possible on specified patterns of energy depositions or multiplicity distribution. This is crucial, since we want to be able to observe effects of the order of 10^{-9}-10^{-10} of all interactions, with a good detection efficiency.

iv) No ambiguity or saturation has to occur up to the highest particle multiplicities.

Our initial consideration had been given to a magnetic field detectors. However, complications with neutral detection and points (iii) and (iv) above have led us to consider instead a calorimetric device, inside which the whole hadronic and electro-

Another very attractive possibility consists of making use of the Cerenkov radiation from purified water. Our Monte Carlo calculations shown that $\sim$ 75 % of the energy lost by a nuclear cascade of few GeV is dissipated by Cerenkov active particles. In this case the cost of the radiator is practically nil. It may be convenient to add a wave shifter, like quaterphenil in very tiny quantities (10^{-3}-10^{-4}) in order to recover the ultra-violet fraction of the spectrum. An 88 ton detector has been reported in the literature[13] years ago. The counter, a cylinder $\sim$ 4.75 m in diameter and 5 m in depth, was equipped with only 16 photomultipliers (PM's), i.e. 1 PM for each 7 m^2 of counter surface. Approximately 23 photoelectrons were recorded for relativistic muons, producing $\sim$ 1 GeV of energy loss. Straightforward improvements, i.e. adding wave shifter and doubling the active PM's surface could increase the yield to 70-80 photoelectrons/GeV. For comparison, the Harvard-Penn-Wisconsin ν-detector[12] with 196 PM's and 96 tons of saturated mineral oil scintillator has a yield of $\sim 10^4$ photoelectrons/GeV. Normalized to the same active PM surface, we expect (16 x 2/196) x 10^4 = 1.6 x 10^3 photoelectrons/GeV, or from the scintillator $\sim$ 30 times more light than from the Cerenkov radiator.

TABLE 1

Cost versus light yield for mineral-based oil

Fraction of organic solvent	8%	20%	40%
Light yield, normalized to anthracene	0.15	0.35	0.43
Light yield, photons/GeV	6 x 10^5	1.4 x 10^6	1.7 x 10^5
Cost (100 tons)	320 \$/t	500 \$/t	800 \$/t

Note : It is very likely that for larger quantities prices could be further reduced.

TABLE 2

Parameters of steel-sandwich counters

	Case A	Case B	Solid steel block
Plate thickness	1 cm	2 cm	-
Liquid scintillator	1 cm	1 cm	-
Average lengths			
a) collision	20.8 cm	17.3 cm	12.9 cm
b) radiation	3.39 cm	2.60 cm	1.77 cm
Fraction of energy dissipated in the liquid	0.155	0.084	-
Total stack for 10 coll. lengths:			
a) thickness	2.08 m	1.73 m	1.29 m
b) specific weights			
i) scintillator	104 g/cm^2	57.66 g/cm^2	
ii) iron	818 g/cm^2	907 g/cm^2	
iii) total	922 g/cm^2	965 g/cm^2	1015 g/cm^2
c) number of plates	104	57	-

The third alternative is the steel-scintillator sandwich. If the minimum distance from the interaction point is chosen to be 1 m, the minimal mass required for 10 collision lengths is $\sim$ 546 tons for the choice of 2 cm steel plates (case B of Table II), made of 513 tons of steel and 33 tons of high grade scintillator. However, since light pipes have to come out on the sides and the counter has to be finely subdivided, we have to add a considerable overlap factor and increased average distances. We have tried several solutions and found that an overhead factor $\sim$ 1.6 is a realistic estimate. Consequently we end up with $\sim$ 820 tons of steel and 52 tons of high-grade scintillator. At standard prices, the cost of the raw materials will amount to approximately 540,000 $ for the steel and 41,600 $ for the liquid. The surface of the steel plate reaches the fantastic figure of 9339 m^2!! Aside from the size, complexity, and cost of the device, the performance may turn out to be rather marginal. Fluctuation in excess of the energy lost in some of the liquid scintillators could bring a fraction of the very numerous, low (transverse) momentum events to overflow into the high momentum bins.

The total absorption counter is superior on this point, since, provided a reasonable thickness and uniformity are guaranteed, there can be no energy deposit greater than the full containment. Furthermore since the medium is transparent, light is collected by phototubes behind the cascade and adjacent cells are separated by simple optical screens. The liquid is held in a simple, almost spherical container centred around the interaction point. Ten collision lengths require $\sim$ 650 tons of liquid, which is less than the steel of the scintillator-steel sandwich at a lower unit cost. The cost of the low-grade liquid is $\sim$ 200,000 $ (0.780 MSF). Actually detailed Monte Carlo calculations (see Section 4) indicate that, apart from a narrow cone in the forward direction, $\sim$ 4.5 m of liquid are sufficient. Then the volume drops to 550 tons and the cost to 175,000 $ (628,000 SF). The possibility of using a Cerenkov water-radiator is of course very attractive,

since the price of the radiator is negligible, and an even better containment can be obtained by increasing the weight of the calorimeter to $\sim 10^3$ tons. Of course some of the saving is absorbed by the increased number of PM's and by some increased difficulties in the light collection because of the lower (n = 1.333) refractive index. In the following we choose the low-grade liquid scintillator, for which the technology is well in hand. The possibility of a Cerenkov radiator remains a further option, requiring additional tests.

Because of the unconventional nature of the detecting apparatus and its large size, we discuss briefly some of the technical points. They are closely inspired by the experience of the NAL calorimeter of the Harvard-Penn-Wisconsin group[12].

The container is a large steel sphere. Windows for the PM's are plexiglas ports on flame-cut round holes. The PM bases are designed so as to contain the liquid in case of an accidental collapse of the window.

Light collection is based on internal total reflection. Walls of the container are covered with a very thin foil (1 mil) of teflon FEP. The refractive index of FEP is 1.33, lower than that of the liquid which is ~ 1.50. Consequently, total reflection takes place in the transition between the liquid and the plastic coating (Fig. 5). The limiting angle is $\sim 26^{\circ}$. For increased reflectivity of the light outside the total reflection cone, the side of the FEP not in contact with the liquid is aluminized. The method has proved itself fully successful at NAL[12].

Separation between adjacent cells is obtained with thin plastic screens, shaped as hexagonal prisms. A light-collecting cone matches the light from the prism to the phototubes. No appreciable force is acting on the plastic structure, since its density is almost the same as the liquid.

The Harvard-Penn-Wisconsin ν-detector has a surface area of 130 m^2 and 196 PM's or 1.56 PM's/m^2. The light collection is ∿ 100 keV/photoelectron. For the present application a considerably less efficient light collection is largely adequate. The light yield is ∿ ¼ due to the lower grade liquid. We assume 1 PM/m^2, corresponding to a collection figure better than 1 MeV/photoelectron. The sphere consists of $4\pi \times 5^2 = 314$ PM's. Apart from a few cells around the beam pipes, the bulk of PM's are slower, (< 100 $ each) tubes.

We consider the inner-core sphere as inaccessible without emptying the large container. The maximum reliability is then required for all components.

4. FURTHER REMARKS ON THE CALORIMETER. THE ANGULAR AND THE ENERGY RESOLUTIONS.

We have made use of the experimental data on nuclear cascade[11] and of Monte Carlo calculation[14] in order to estimate the containment of energy of the nuclear cascades inside the calorimeter. The Monte Carlo and the experimental results are in fairly good agreement although the Monte Carlo gives a systematically lower containment than the experiment (Figs. 6,7). Calculations are giving in general a pessimistic estimate of the energy resolution. The main assumptions behind the calculations[14] are as follows :

i) The ionization energy loss is correctly distributed along the paths.

ii) Secondary particles of energy below E_{th} ∿ 50 MeV are assumed to stop immediately.

iii) Neutral π mesons have the same distribution as charged ones. The γ-ray energy is deposited according to the interpolations of measured or calculated curves.

iv) A very approximate description of the energy lost by nuclear de-excitation is given : one third of the energy is assumed deposited within the bin where the interaction has taken place, while the rest is deposited isotropically with a interaction length of 50 MeV neutrons.

v) $\pi \rightarrow \mu$ decay is taken into account.

The main source of uncertainties in the calculations comes from item iv).

The energy containment is rather independent of the energy and it is shown in Fig. 8 for single particles. The typical value is 15 ÷ 20 % FWHM, largely sufficient for our present purposes. Since the energy resolution is independent of energy, the resolution for a jet of several particles is considerably better than for single particles. This is illustrated in Fig. 9, where we have given the energy containment distribution of a jet of total energy E_{TOT} = 15 GeV, invariant mass $\sim$ 6 GeV, decaying according the Hagedorn-Ranft thermodynamical model.

The angular resolution inherent in the hadronic cascade is shown in Figure 10, calculated for a single particle of 10 GeV/c momentum. Results are in agreement with experimental observations. The angular distribution is also an almost energy independent function.

Let us consider some further questions related to the expected performance of the calorimeter.

1. Non-linear response of the scintillator. One of the properties of almost all scintillating materials is that saturation phenomena reduce the light output for very densely ionizing particles. Typically a 1 MeV proton could give only $\sim$ 1/3 of the light output and a 5 MeV alpha-particle $\sim$ 1/10. Fluctuations in the number of heavy ionizing particles could give rise to

some loss of resolution. Monte Carlo calculations provide some guidance and give supporting evidence to the fact that the fluctuations in the fraction of energy lost by slow particle should be small. However, it could cause differences in behaviour between hadronic and electromagnetic showers, since for the latter only a minor fraction of the energy goes into densely ionizing tracks. We plan to investigate further these points experimentally.

2. Non-uniform light collection. Sometime events may deposit anomalous amounts of energy just in front of the phototube giving an anomaly to the high side of the resolution curve. In order to overcome the effect we intend to fill up the reflecting cone around the phototubes with pure mineral oil, rather than scintillator. A thin transparent mylar foil separates the two sections.

3. Collecting times for slow neutrons. A fraction of the energy is dissipated in the form of slow neutrons. Although this energy would be eventually collected, the delay due to the slow velocities may exceed the resolving time. Therefore, some of our energy resolution may have to be sacrificed as a trade for the speed of response.

4. Energy calibration. An important problem is the stability and energy calibration of the many cells of the calorimeter. We plan to use several methods. A first one consists of light emitting diodes. The method is good for fast check-up. We intend to locate the diodes at the boundary between three cells, so that light from each source is sent to all three neighbouring cells. It is possible to link the given gain between tubes without requiring constant light output from the light emitting diodes. A second form of calibration, very effective in view of the large size of the detector are (cosmic-ray) muons. The counters of the central region, and the requirement of only two back-to-back cells have

given pulses, define reasonably well the direction of the muons. Thridly, every beam-beam event is expected to deliver the full energy in the calorimeter (56 GeV line).

5. EVENT SELECTION AND IDENTIFICATION

Selection criteria are generated on-line in order to reduce the events rate $> 10^5$/sec to the level of $\sim 10^2$/sec which can be recorded by a video tape. We can apply several kinds of selection criteria :

i) The total visible energy must be compatible with twice the ISR beam energy. This simple mixing and discrimination operation rejects single beam background and cosmic rays.

ii) The distribution of the energy depositions must satisfy to specified criteria. This is easily performed in an analogic form, mixing the pulses from cells weighted through specific attenuation networks. For instance the $p_\perp$ delivered to each cell is evaluated introducing attenuation proportional to $< \sin \theta_{CM} >$. Adding $p_\perp$ signals with opposite signs for the upper (left) and lower (right) hemispheres provides the transverse momentum unbalance in the up-down (left-right) direction. Adding all $p_\perp$ signals with the same sign measures the total transverse momentum for each event. Diode mixing can be used in order to determine the largest amongst a set of signals.

iii) Multiplicity of cluster structure can be selected from the central, inner detector.

After event selection, the following information is recorded on to tape for the off-line analysis programs :

i) The spatial distribution of all tracks coming out of the interaction, as detected by the central, inner core chambers.

ii) The angular distribution of γ-rays, identified by their conversion in the lead-glass honeycomb hodoscope in the inner detector.

iii) The distribution of energy dispositions over the calorimeter sphere.

An important form of potential background is represented by accidental pile-up of two or more events within the resolving power of the detector. Assuming 10^5 events/sec, the probability of an accidental time coincidence within $\sim$ 20 ns is $\frac{1}{500}$, or 200 events/sec. Spatial coincidence of tracks to a common vertex within $\sim$ 1 mm^3 gives another powerful factor, i.e. $10^{-3} \times \frac{1}{100} = 10^{-5}$, since the volume of interaction is $\sim$ 100 cm^3. The accidental rate is at this level still $\sim$ 7 events/hour. In order to further reduce this number we must make use of the energy information of the calorimeter. For instance beam-beam pile-up delivers to the calorimeter twice the expected amount of energy.

Beam-gas piled up with beam-beam events are removed as well by the visible energy requirement. Two simultaneous beam-gas interactions cannot be separated by the visible energy : however they are less probable and, at least under normal vacuum conditions, are removed by the timing and geometry cuts. Finally beam-gas are strongly rejected by specific event selection criteria, like large $p_\perp$ or large multiplicities. The expected number of accidental events can be evaluated "a posteriori" from space and timing informations on tape.

6. CONCLUDING REMARKS

The proposed detecting apparatus possesses to our opinion remarkable potentialities : its genuine 4π geometry, neutral detection, and its ability of extracting significant

information up to the highest particle multiplicities. Several fundamental physical quantities, like the energy and transverse momenta distributions, are directly accessible to a very fast decision-making electronics. These features are helping very significantly in the selection of cross sections of order $10^{-34} \div 10^{-36}$ cm^2 where many exciting new phenomena are postulated.

We believe that the calorimeter of the type described is completely complementary to the large 4π magnetic analysis (SFM) detector. In spite of its unusual size, the construction of the detector is relatively straightforward and it requires no development of new technologies. The large sphere is filled with a rather inert and unexpensive type of mineral oil. Finally the experience that some of us have gained in the construction of the 100-ton liquid scintillation calorimeter at NAL gives confidence for the presently proposed extrapolation.

We are in the process of defining the time-table for the detailed design, construction and installation. The installation of the large steel structure must be carried out during a long machine shut-down (January 1974). A preliminary investigation indicates I1 as the most suitable interaction region.

Some parasitic time at the PS is required in order to test prototypes of the calorimeter and of the chambers of the inner core.

FIGURE CAPTIONS

Fig. 1 : Electromagnetic contribution to proton-proton inelastic scattering.

Fig. 2 : Point-like electromagnetic scattering cross section (Mott scattering).

Fig. 3 : Experimental set-up.

Fig. 4 : Details of the inner detector.

Fig. 5 : Principle of the FEP total reflecting surface.

Fig. 6 : Longitudianl energy containment.

Fig. 7 : Transverse energy containment.

Fig. 8 : Distribution of the energy containment, calculated according to Ref. 14 for single particle incident on the calorimeter.

Fig. 9 : Distribution of the energy containment for hadronic cascade of p_{tot} = 15 GeV, Mass = 6 GeV.

Fig. 10 : Angular resolution for a single 10 GeV particle.

REFERENCES

1. For the most recent results on NAL experiments, see for instance the rapporteur's talks to the Batavia Conference (Sept. 1972) by M. Jacob and G. Giacomelli.

2. E.D. Bloom et al., SLAC Report No : SLAC-PUB 796 (1970)

3. See for instance the rapporteur talk to the Batavia Conference (Sept. 1972) by D. Perkins, also for earlier references.

4. F.R. Low and S.B. Trieman, "Electromagnetic contributions to Hadron processes, CRISP 71-37 and Physical Review Comments, 1971.

5. S.M. Berman, J.D. Bjorken, J. Kogut, "Inclusive Processes at High Transverse Momenta", SLAC Preprint (1971).

6. We are indebted to Professor C.N. Yang for this comment.

7. S. Berman and M. Jacob, Phys. Rev. Letters 25, 1683 (1970).

8. J.J. Sakurai, UCLA preprint 1972.

9. For review see : D. Lukey, in Proc. Int. Symposium on Electron and Photon Interaction at High Energies, Hambourg (1965). (Springer Verlag, Berlin 1965), p. 397.

10. M. Holder et al., A High Resolution Total Absorption Spectrometer for simultaneous Detection of Several High Energy γ-rays, submitted to Nuclear Instruments and Methods, 8 Sept, 1972.

11. B. Huges et al., Nuclear Instruments and Methods 75, (1969) 130-136.

12. Harvard Pennsylvania-Wisconsin proposal, NAL, # 1A (unpublished).

13. V.L. Dadykin, Pribory j Teknika Exsperimenta N1, 60 (1972).

14. J. Ranft, Nuclear Instruments and Methods 81, (1970) 29÷35.

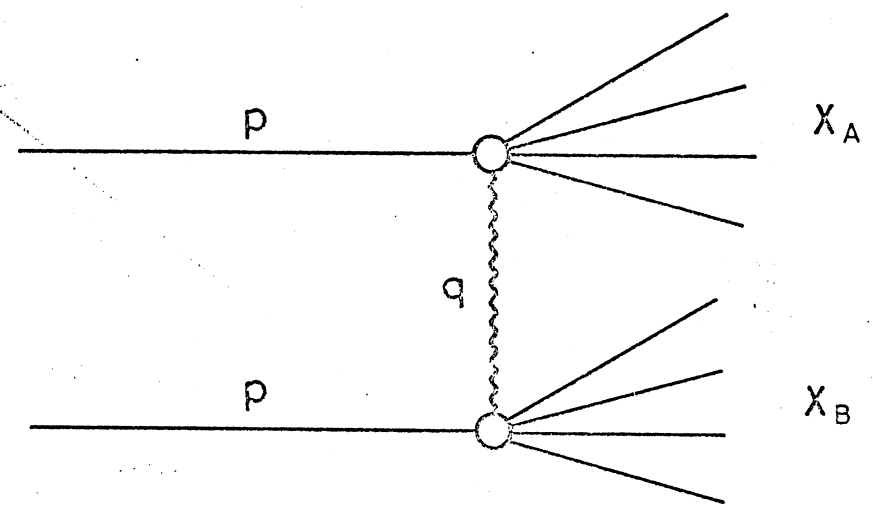

Electro - magnetic p - p scattering diagram

FIG.1

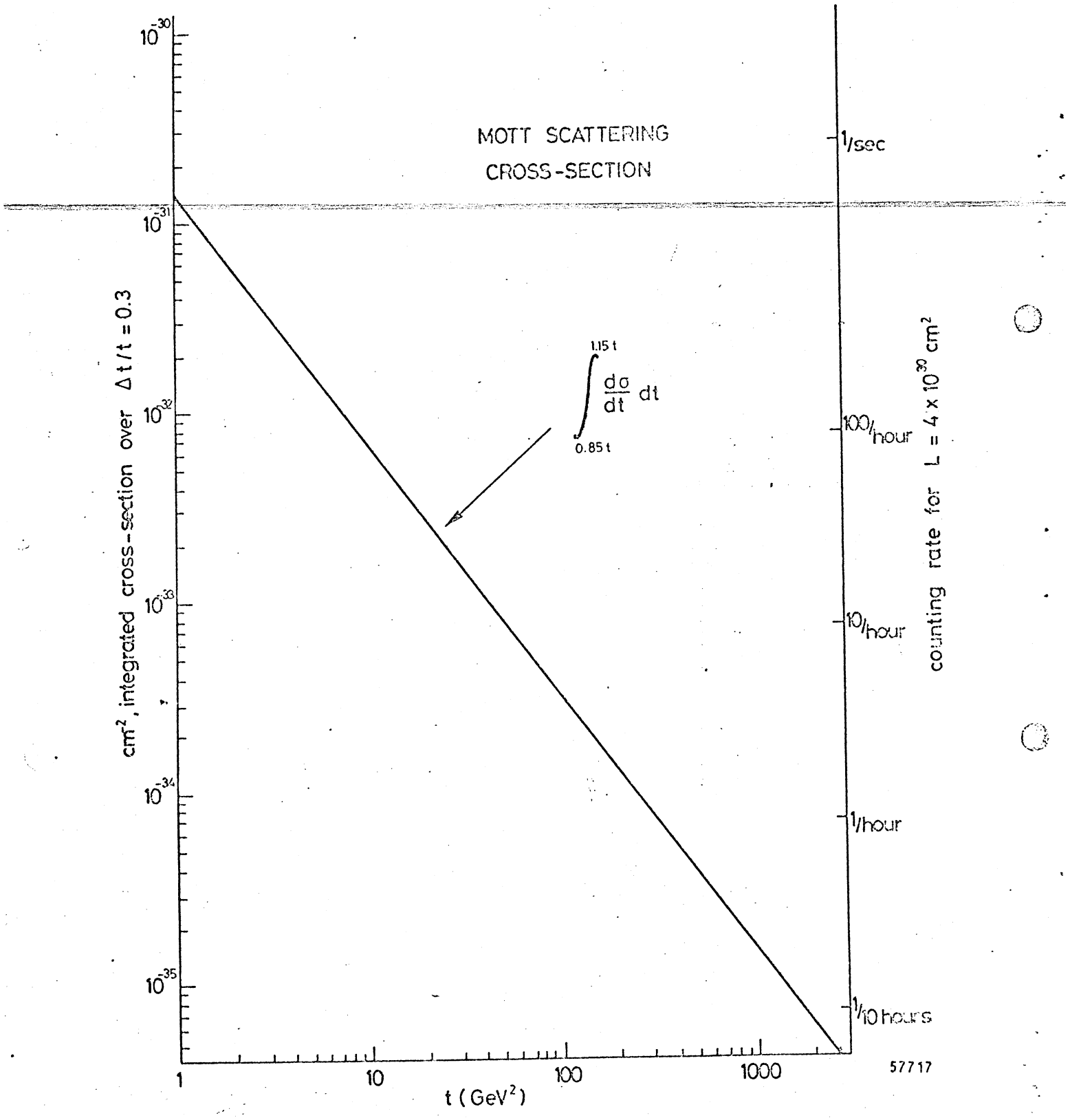
MOTT SCATTERING
CROSS-SECTION
10^{-30}
10^{-31}
10^{-32}
10^{-33}
10^{-34}
10^{-35}
cm^{-2}, integrated cross-section over $\Delta t/t = 0.3$
1.15 t
$\int \frac{d\sigma}{dt} dt$
0.85 t
1/sec
100/hour
10/hour
1/hour
1/10 hours
counting rate for $L = 4 \times 10^{30}$ cm^{-2}
1
10
100
1000
t (GeV^2)
57717

FIG. 2

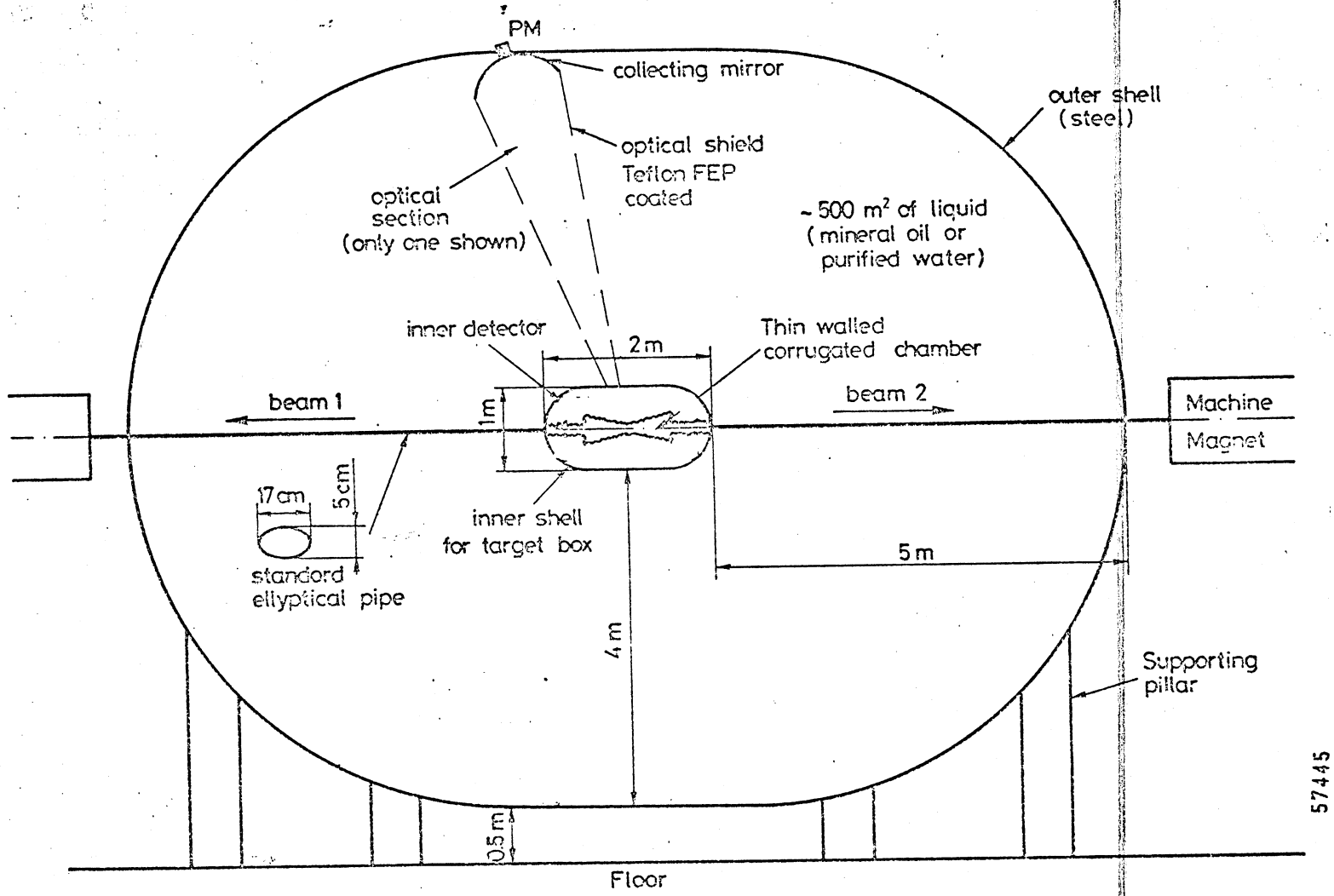
PM
collecting mirror
outer shell
(steel)
optical shield
Teflon FEP
coated
optical
section
(only one shown)
~ 500 m² of liquid
(mineral oil or
purified water)
inner detector
2 m
Thin walled
corrugated chamber
beam 1
beam 2
1m
Machine
Magnet
17 cm
5 cm
inner shell
for target box
standard
ellyptical pipe
5 m
4 m
Supporting
pillar
0.5 m
Floor
57445

FIG. 3

INNER SHELL DETECTOR

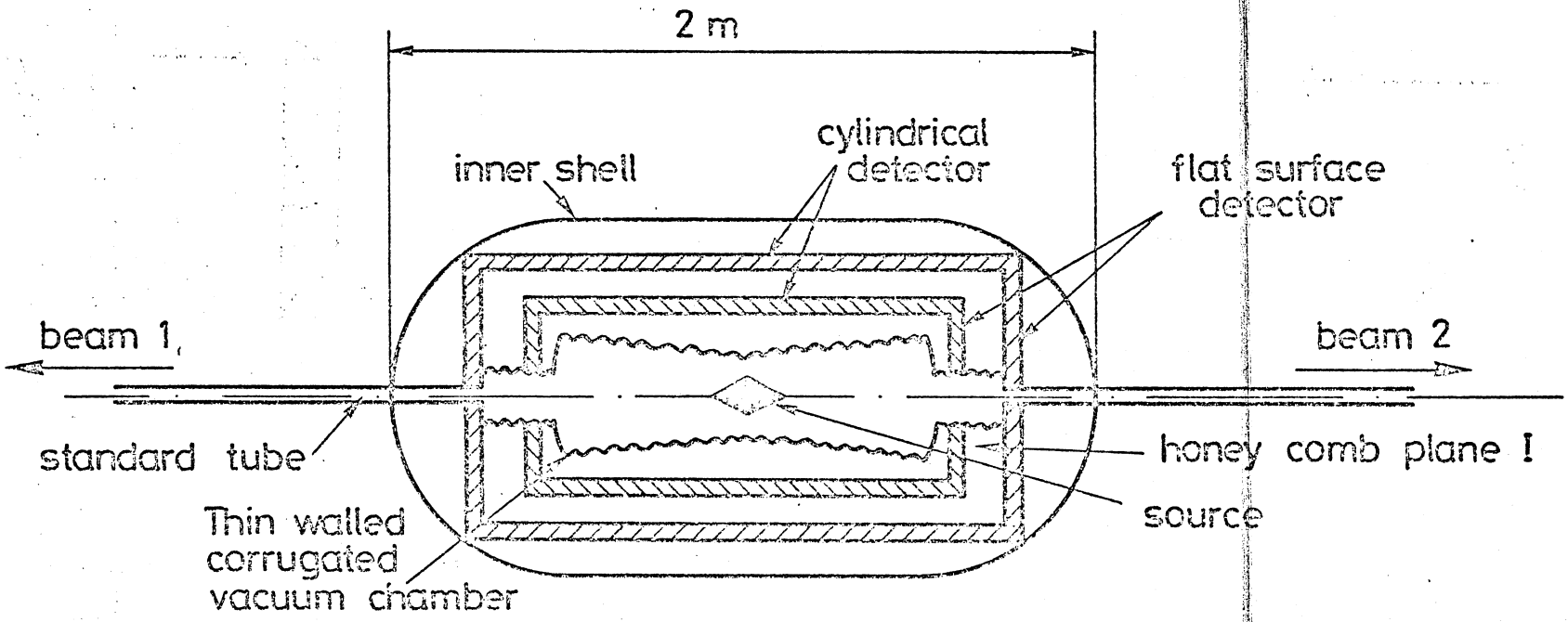

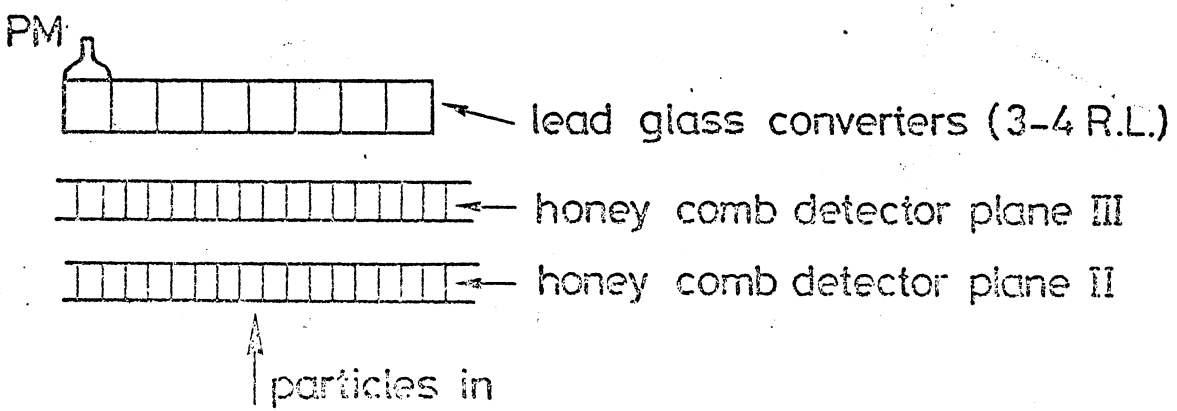

Detail of detector

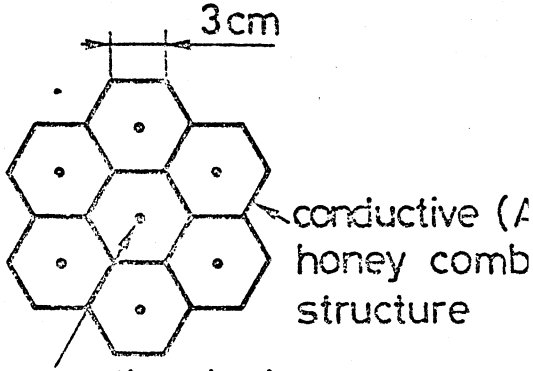

Detail honey comb detector plane

FIG. 4

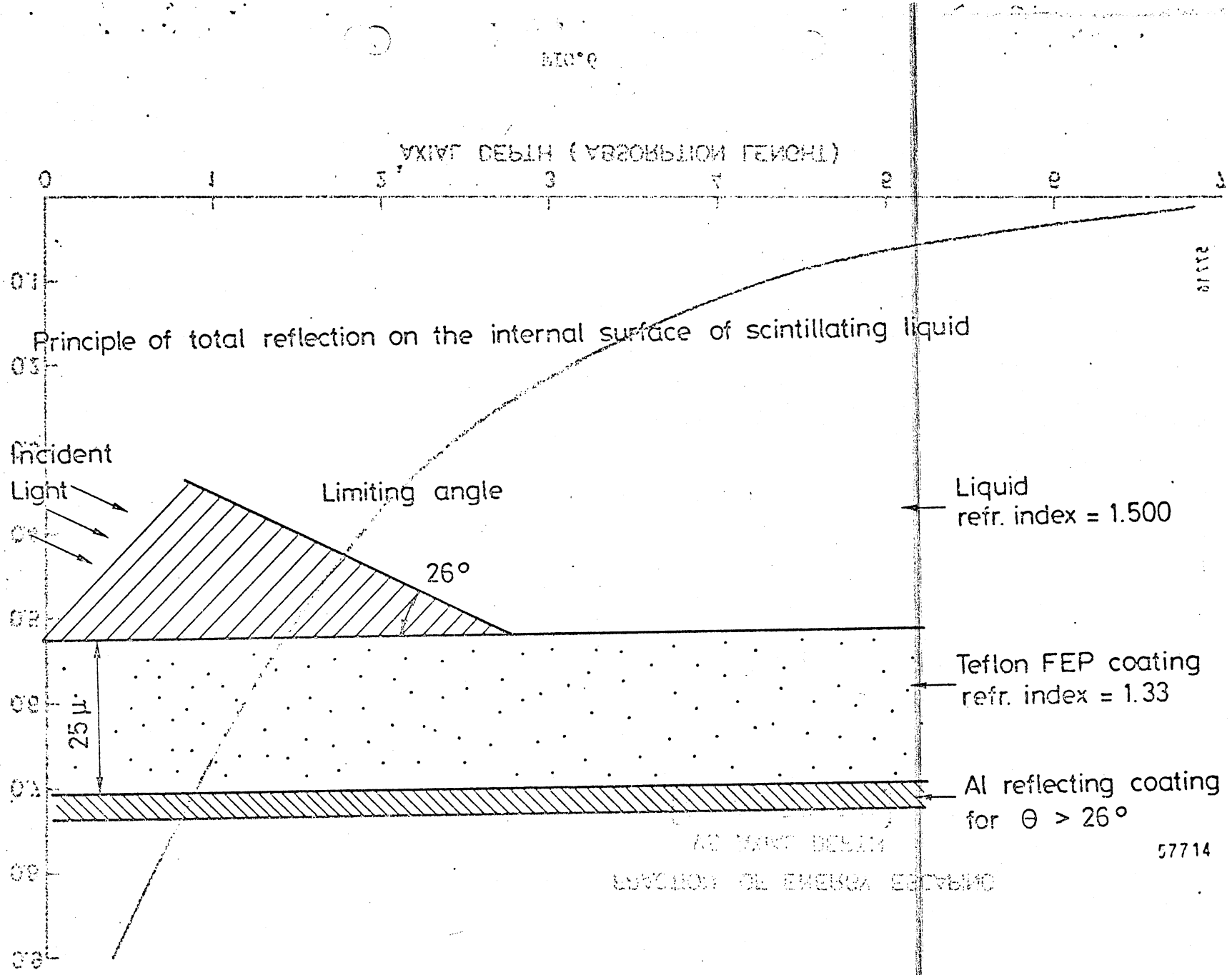
Principle of total reflection on the internal surface of scintillating liquid
Incident
Light
Limiting angle
26°
Liquid
refr. index = 1.500
Teflon FEP coating
refr. index = 1.33
25 μ
Al reflecting coating
for Θ > 26°
57714

FIG.5

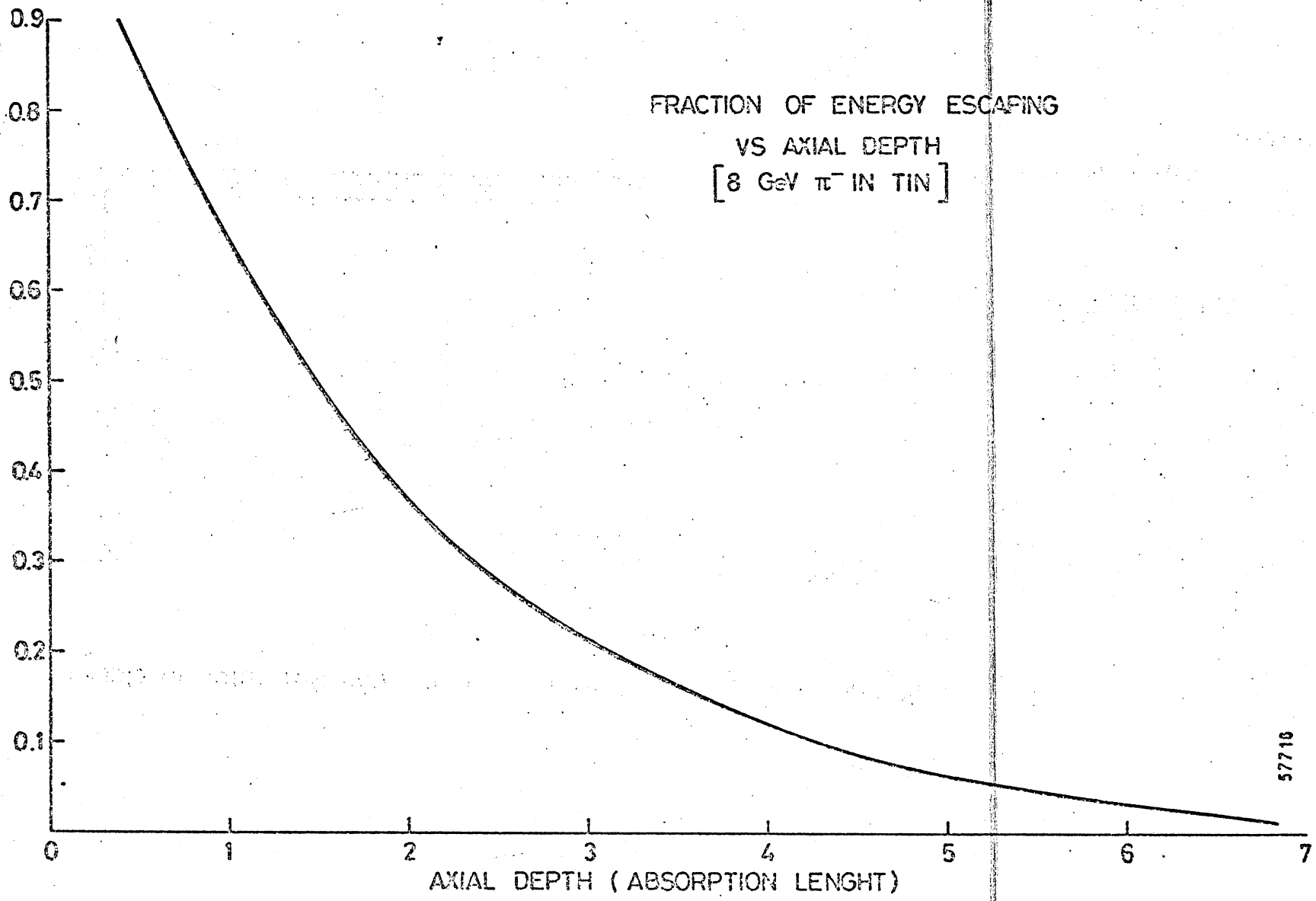
FRACTION OF ENERGY ESCAPING
VS AXIAL DEPTH
[8 GeV π⁻ IN TIN]
0.9
0.8
0.7
0.6
0.5
0.4
0.3
0.2
0.1
0
1
2
3
4
5
6
7
AXIAL DEPTH (ABSORPTION LENGHT)
57710

FIG.6

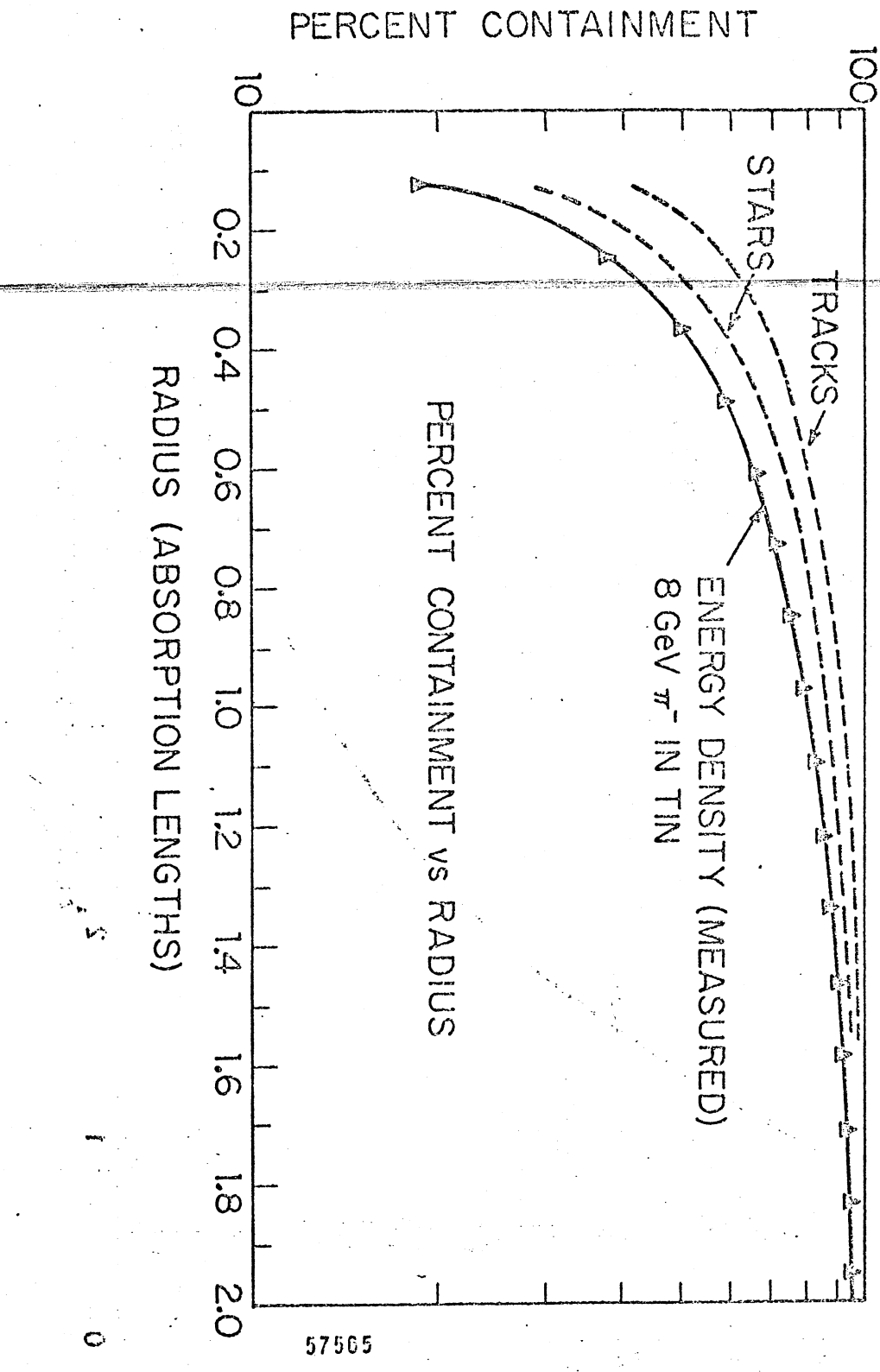
PERCENT CONTAINMENT
100
10
STARS
TRACKS
ENERGY DENSITY (MEASURED)
8 GeV π⁻ IN TIN
PERCENT CONTAINMENT vs RADIUS
0.2
0.4
0.6
0.8
1.0
1.2
1.4
1.6
1.8
2.0
RADIUS (ABSORPTION LENGTHS)
57565

FIG. 7

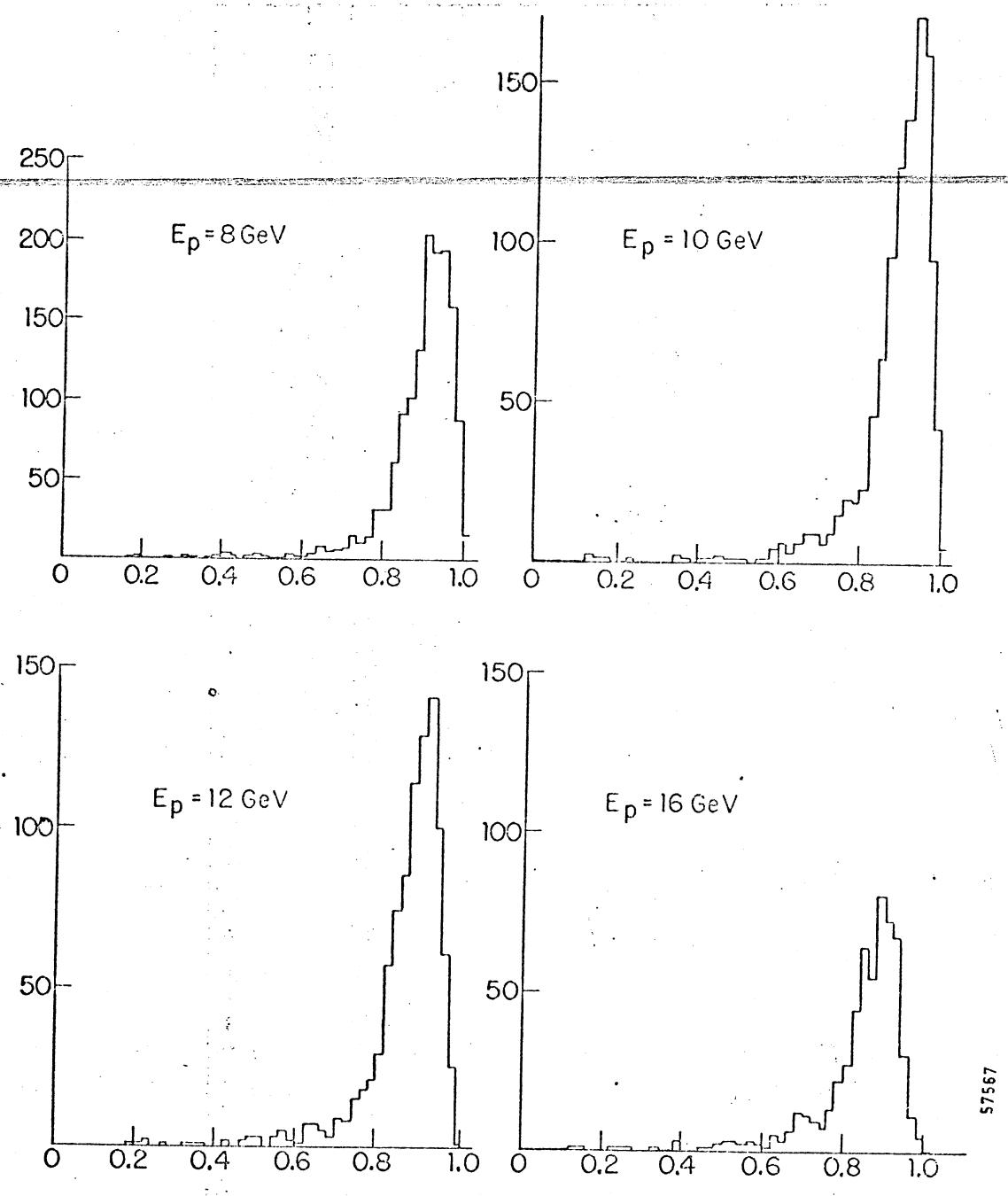
E_p = 8 GeV
E_p = 10 GeV
E_p = 12 GeV
E_p = 16 GeV
0
0.2
0.4
0.6
0.8
1.0
50
100
150
200
250
57567

FIG. 8

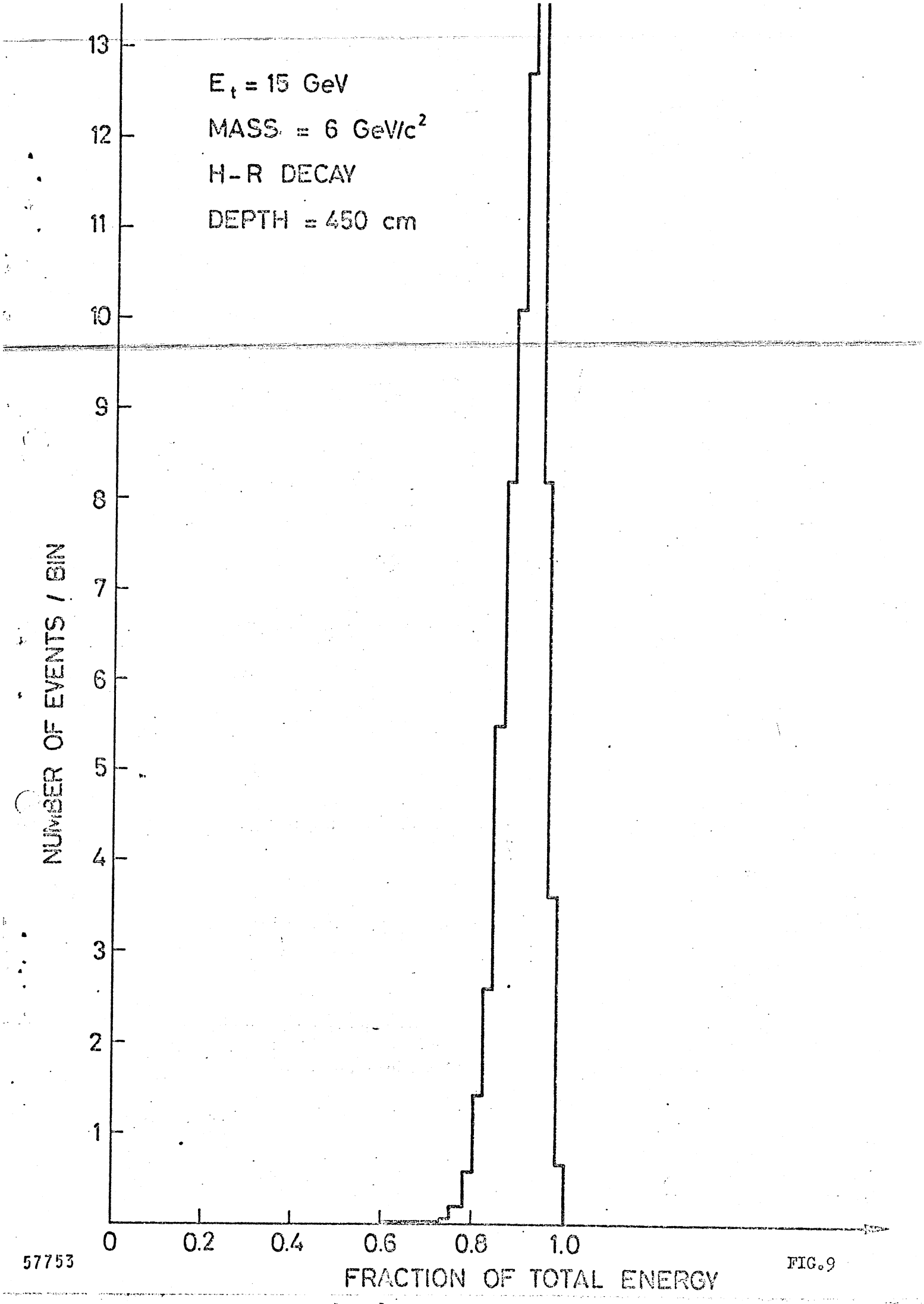
E_t = 15 GeV
MASS = 6 GeV/c^2
H-R DECAY
DEPTH = 450 cm
NUMBER OF EVENTS / BIN
FRACTION OF TOTAL ENERGY
0
0.2
0.4
0.6
0.8
1.0
1
2
3
4
5
6
7
8
9
10
11
12
13

57753

FIG. 9

Contours of equal intensity in liquid scintillator

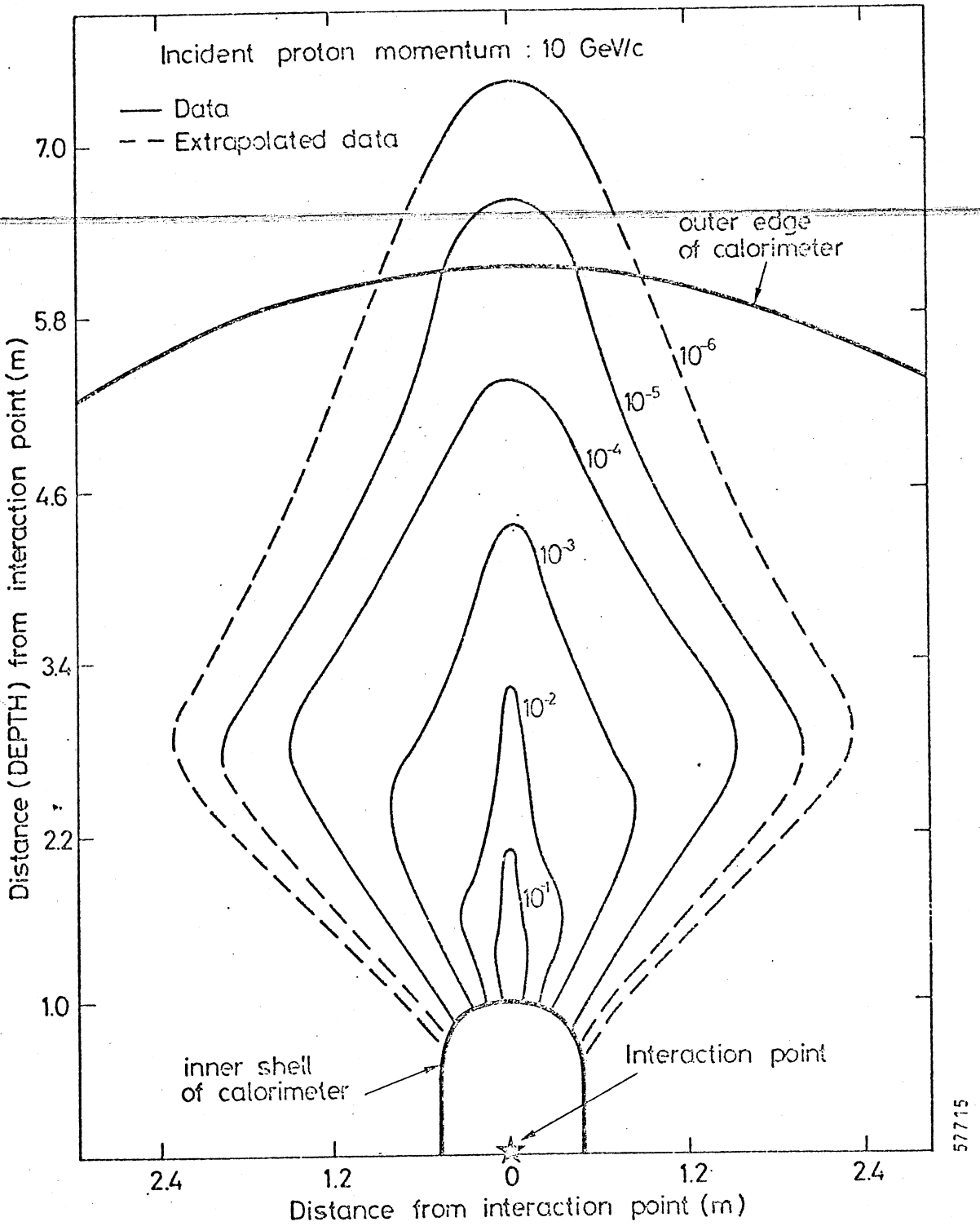

FIG.10